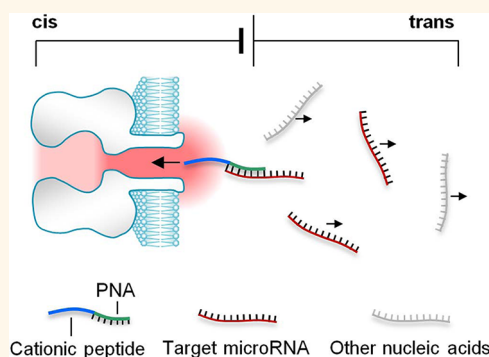# Designing a Polycationic Probe for Simultaneous Enrichment and Detection of MicroRNAs in a Nanopore

Kai Tian,[†] Zhaojian He,[‡] Yong Wang,[†] Shi-Jie Chen,[‡] and Li-Qun Gu[†,*]

[†]Department of Biological Engineering and Dalton Cardiovascular Research Center and [‡]Department of Physics, University of Missouri, Columbia, Missouri 65211, United States

ABSTRACT The nanopore sensor can detect cancer-derived nucleic acid biomarkers such as microRNAs (miRNAs), providing a noninvasive tool potentially useful in medical diagnostics. However, the nanopore-based detection of these biomarkers remains confounded by the presence of numerous other nucleic acid species found in biofluid extracts. Their nonspecific interactions with the nanopore inevitably contaminate the target signals, reducing the detection accuracy. Here we report a novel method that utilizes a polycationic peptide-PNA probe as the carrier for selective miRNA detection in the nucleic acid mixture. The cationic probe hybridized with microRNA forms a dipole complex, which can be captured by the pore using a voltage polarity that is opposite the polarity used to capture negatively charged nucleic acids. As a result, nontarget species are driven away from the pore opening, and the target miRNA can be detected accurately without interference. In addition, we demonstrate that the PNA probe enables accurate discrimination of miRNAs with single-nucleotide difference. This highly sensitive and selective nanodielectrophoresis approach can be applied to the detection of clinically relevant nucleic acid fragments in complex samples.

The nanopore provides a sensitive single-molecule platform for exploring a large variety of life sciences problems.[1−14] Not only are nanopores being widely developed for rapid and low-cost gene sequencing[15−18] but they also have been found to be able to analyze epigenetic changes such as DNA methylation[19] and gene damage.[20] In this rapidly evolving field, the nanopore sensor has recently been designed to electrically detect microRNAs (miRNAs),[21,22] a class of tiny but extremely important regulatory RNA molecules.[23−26] As miRNAs are potential cancer biomarkers,[27−35] an accurate nanopore sensor for circulating miRNA detection would offer a potential noninvasive tool for screening and diagnostics of diseases.

However, translating the nanopore sensor into a clinically usable technology faces challenges due to the complexity of clinical samples. Generally, the clinical samples used to test for miRNA are RNA extractions from a patient's biofluids such as plasma.

These extractions are a complex collection of various RNA species: miRNAs, mRNAs, tRNAs, *etc*. When the nanopore is used to detect the target miRNA, any free nucleic acids in the RNA mixture can also nonspecifically interact with the pore. These interactions result in intensive "contaminative" signals that severely influence the target miRNA determination, and they should be eliminated.

We have devised a solution to this contamination problem (Figure 1): by using a polycationic probe as the carrier, the nanopore can selectively capture and detect the target miRNA. The probe comprises a sequence of peptide nucleic acids (PNA) conjugated with a polycationic peptide lead. The PNA is designed to specifically capture the target miRNA. Upon hybridization, the positively charged peptide lead and the negatively charged miRNA together form a dipole. This structure can be driven into the nanopore by a large electric field gradient around the nanopore opening. At the same
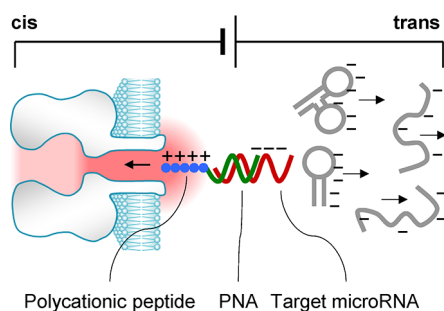
Figure 1. Cationic probe-enabled interference-free detection of miRNAs in the nanopore. The probe comprises a capture domain (PNA, green) attached with a polycationic polymer lead (peptide, blue). The capture domain hybridizes with the target miRNA (red). Under a transmembrane voltage, the miRNA•probe complex is drawn into the nanopore by the electric field gradient at the pore opening, while any free nucleic acids without the probe binding carry negative charges (gray) and electrophoretically move away from the pore.

time, any free nucleic acids without probe hybridization would carry negative charge and migrate away from the pore opening. Consequently, only the signatures for the miRNA•probe complex and probe alone in the nanopore will be identified, and any interference signal originating from free nucleic acids is completely eliminated.

RESULTS AND DISCUSSION

Simultaneous Enrichment and Detection of miRNAs with a Polycationic Probe. We chose the Let-7 tumor-suppressing microRNA family[31,36,37] as the target. Figure 2a and Supporting Information Table S1 show the sequences of Let-7b and its probe P_{7b}. P_{7b} contained a 10 base PNA sequence designed to specifically hybridize with Let-7b. The PNA was extended at the N-terminal with an HIV-1 TAT polycationic peptide,[38] which includes six arginines and two lysines, which are positively charged amino acids. All analytes, including the miRNA, the probe, and their mixtures, were presented on the trans side of the nanopore. A positive voltage was applied from the trans side to the grounded cis side. This voltage polarity can drive cationic molecules toward the pore, while repelling anionic molecules away from the pore. We utilized the mutant α-hemolysin pore K131D as the sensor because the seven negatively charged Asp131 residues at the trans opening of this mutant pore can enhance the attraction of cationic molecules.

We found that the current trace for Let-7b alone in trans solution (Figure 2b, +180 mV) was similar to that in the absence of any nucleic acid analyte (Figure S1), indicating that Let-7b never blocked the pore itself without hybridization. This absence of Let-7b blocks is expected given that the positive voltage should prevent the negatively charged miRNA from interacting with the nanopore. In contrast to Let-7b, the current trace for P_{7b} alone in trans solution shows a large number of level 1 blocks (Figure 2c). The duration of

these blocks τ_{off} was 4.8 ± 1.2 ms, and their relative conductance I_R/I was 8.2% (I_R and I are currents of the block and the empty pore, Figure 2e). The presence of these level 1 blocks is expected given that the positive voltage should lead the positively charged probe toward the pore. When the Let-7b/P_{7b} mixture was added in trans solution, the level 1 blocks were rarely observed. Instead, we identified a large number of distinct level 2 blocks (Figure 2d). Compared with the level 1 blocks, the level 2 blocks were 6-fold longer with a duration of 28 ± 4 ms and featured higher relative conductance with I_a/I = 26% (Figure 2e). These level 2 blocks cannot be observed at negative voltage. Because the level 2 blocks were only observed in the presence of both Let-7b and P_{7b}, they are attributed to the formation of Let-7b•P_{7b} hybrids that interact with the pore's trans opening. Therefore, the level 2 blocks serve as signatures for Let-7b identification.

To validate this finding in a more complex system, we mixed Let-7b with two background RNAs, miR-155 and miR-21, which have significantly different sequences from Let-7b. Indeed, no block was observed for Let-7b in the presence background RNAs (Figure 2f, +180 mV), suggesting that none of nucleic acid components can interact with the pore at this voltage. In the presence of P_{7b} in the mixture, a large number of level 2 blocks appeared (Figure 2g). As the background RNAs cannot hybridize with P_{7b}, the level 2 blocks should be attributed to the Let-7b•P_{7b} hybrids. Their properties, including the current amplitude, duration, and occurring frequency (Figure 2h and Table S2), had no significant difference from that observed without background RNAs (Figure 2c), suggesting that the background RNAs do not affect the target miRNA detection. Therefore, we conclude that a polycationic probe can electrically separate the target miRNA from free nucleic acid components. The probe-labeled miRNAs can be enriched around the nanopore and simultaneously detected. As free nucleic acids not bound to complementary probes cannot interact with the pore under these conditions, their affect on signature recognition is effectively eliminated.

Configuration of the miRNA•Probe Complex in the Nanopore. Since the probe P_{7b} (1.1 nm wide, Figure 3a, left) is narrower than the α-hemolysin pore (1.5−2 nm),[39] the entire polymer including the PNA domain can be trapped in the pore to generate the level 1 block (Figure 3b). PNA itself is rarely trapped in the pore (Figure S1), so the trapping of P_{7b} would likely be led by P_{7b}'s peptide domain. Interestingly, the level 1 block reached the longest duration at +140 mV and was shortened by either decreasing or increasing the voltage (Figure 3g). This "hill"-shaped voltage dependence suggests that P_{7b} binds in the pore. Lower than the peak voltage, P_{7b} tends to return to trans solution from the binding site, and higher than this voltage, P_{7b} traverses the pore to cis solution. It is likely
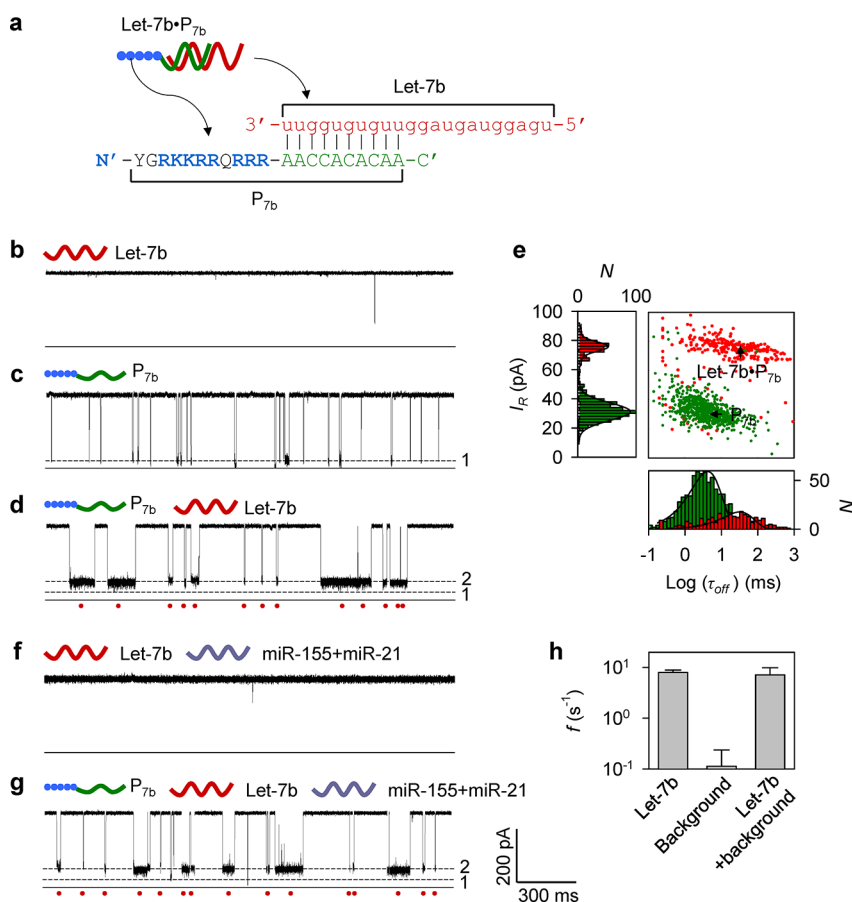
Figure 2. Detection of miRNA with a polycationic probe. (a) Sequences of the target miRNA Let-7b and the polycationic peptide-PNA probe P_{7b}. **(b−d)** Current traces for the K131D pore in the presence of (b) Let-7b alone, (c) P_{7b} alone, and (d) Let-7b/P_{7b} mixture, recorded at +180 mV in 1 M KCl solutions (pH 7.2). Concentrations of Let-7b and P_{7b} were 300 and 100 nM, respectively. **(e)** Scattering plots and histograms showing the duration and residual currents of P_{7b} and Let-7b•P_{7b}. **(f,g)** Current traces for (f) Let-7b and (g) Let-7b/P_{7b} mixture in the presence of background RNAs including miR-155 and miR-21, at +180 mV in 1 M KCl solutions (pH 7.2). Concentrations of Let-7b, miR-155, and miR-21 were 300 nM, and P_{7b} was 100 nM. **(h)** Comparison of frequencies of Let-7b•P_{7b} signatures in the absence of background, the background alone, and Let-7b•P_{7b} in the presence of background.

that the binding of P_{7b} is contributed by PNA interaction with the pore since peptide sequences alone simply translocate through the pore (Figure 3g).

Structural comparison suggests that the folded peptide domain (∼1.7 nm wide) of the Let-7b•P_{7b} complex can enter the pore from the trans opening (∼2 nm), but the Let-7b•PNA duplex (∼2.3 nm wide) is too wide and cannot enter the pore. So the level 2 block is likely generated by the unbound peptide domain occupying the β-barrel stem, which produces a partial block in the ionic current (Figure 3c). The trapped Let-7b•P_{7b} complex is simply released back to trans solution rather than translocate through the pore because the level 2 duration was consistently extended with increased voltage (Figure 3g). Other than level 2 signatures, it was very rare to observe a multilevel block featuring a conductance transition from level 2 to level 1 (Figure 3d). This two-level block represents the unzipping of Let-7b•P_{7b}: its peptide domain first enters the pore for level 2; once unzipped, the dissociated P_{7b} slides into the pore to produce a stepwise change in

conductance to level 1, while the dissociated Let-7c miRNA returns to trans solution. Additional support that the peptide domain is being trapped in the pore comes from observations made using the HIV-TAT peptide. This peptide is the same as our probe peptide. TAT translocation reduced the pore conductance to I_R/I = 27% (Figure 3e), very close to level 2. We further encapsulated the TAT peptide in the mutant pore M113R to confirm this configuration (Figure 3f). In this case, the block duration was consistently extended as the voltage increased (Figure 3g), suggesting that the TAT peptide cannot pass through the M113R pore, but is encapsulated within the β-barrel between the arginine ring and trans entrance. Ultimately, the TAT peptide trapped in this position produced a partial block in conductance at 34%, which is similar to our system's level 2 block in the K131D pore. Therefore, we conclude that the level 2 block represents a β-barrel blockage by the single-stranded folded peptide domain of the probe.

Mechanism for Probe-Induced Nucleic Acid Separation in Electric Field. The core finding in the above study is that
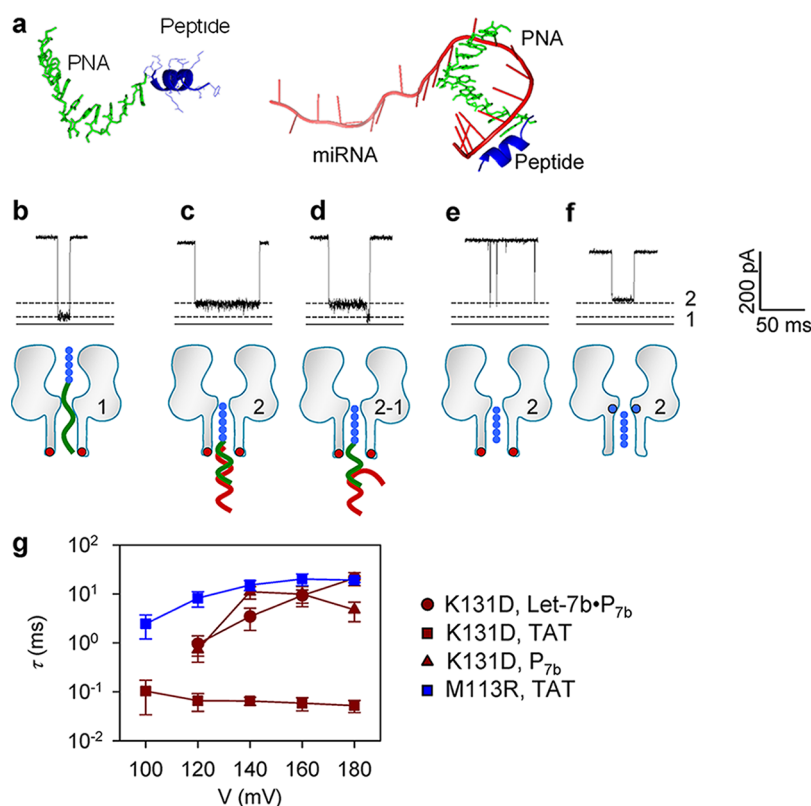
Figure 3. Molecular configurations for various polymers in nanopores. (a) Most stable structures of P_{7b} (left) and the Let-$7b \cdot P_{7b}$ complex (right) in 1 M KCl at pH 7.0. Simulation is detailed in Supporting Information S1. **(b–d)** Typical signature blocks and molecular configurations for trapping of **(b)** P_{7b} (peptide-PNA), **(c)** Let-$7b \cdot P_{7b}$ complex (back to trans solution), and **(d)** Let-$7b \cdot P_{7b}$ complex (unzipped upon trapped) in the K131D pore. **(e)** Translocation of the HIV-TAT peptide through the K131D pore. **(f)** Trapping of the HIV-TAT peptide in the M113R pore. Red dots in the K131D pore (b–e) represent the anionic D131 ring at trans opening, and blue dots in the M113R pore (f) mark the cationic R113 ring in the constrictive region. **(g)** Voltage-dependent duration (τ) of blocks in panels b–f. Red circle: Let-$7b \cdot P_{7b}$ complex in the K131D pore. Red square: TAT peptide in the K131D pore. Red triangle: P_{7b} probe in the M113R pore. Blue square: TAT peptide in the M113R pore.

the free nucleic acids are kept out of the pore while miRNA•probe complexes can enter the pore. This enables interference-free detection of target miRNA using the nanopore platform. However, the mechanism for miRNA•probe capture by the pore is under debate. The charges on the miRNA and the probe are $-22e$ and $+8e$, respectively. Although the effective charges can be greatly lowered in high salt concentration,[40,41] the overall charge polarity retains a net negative charge without inversion.[42] This is in agreement with the zeta-potential (ζ) of the two polymers, $\zeta = -14.4 \pm 1.9$ mV for Let-7b and $+11.7 \pm 0.4$ mV for P_{7b}. Furthermore, we measured the ζ-potential of the Let-$7b \cdot P_{7b}$ hybrid to be -10.0 ± 3.6 mV, confirming that the miRNA•probe complex is negatively charged. Therefore, the negatively charged complex's movement is somehow in the opposite direction from the movement of the other negatively charged RNA species. This phenomenon is inconsistent with either electrophoretic[12,17,41,43] or electroosmotic effect[44−46] explanations for the capturing of this analyte in the nanopore.

We reason that it is the particular distribution of the electrostatic potential at the trans entrance of the nanopore that enables the capture of the miRNA•probe complex. Molecular dynamics simulations have shown that the major drop of the electrostatic potential in the α-hemolysin pore occurs near the nanocavity/β-barrel junction, and the electric field sharply decays within a very short distance ($\sim$1 nm) outside the nanopore.[47,48] The miRNA can diffuse toward the trans entrance up to this distance without feeling the effect of the transmembrane potential. However, once inside that distance, complexes with the positively charged peptide oriented closer to the pore may be captured and drawn into the nanopore. Once in the equilibrium configuration (Figure 1), the transmembrane potential acting on the peptide counterbalances repulsion between miRNA and the negatively charged trans end of the β-barrel. Overall, the highly asymmetrical distribution of charges within the complex coupled with the highly asymmetrical electric field along the pore's axis can allow for a net force pulling the complex into the pore even though the electrostatic simplification of this system would suggest otherwise.

PNA-Enabled Specificity for Single-Nucleotide Discrimination. Both functional explorations and diagnostic applications
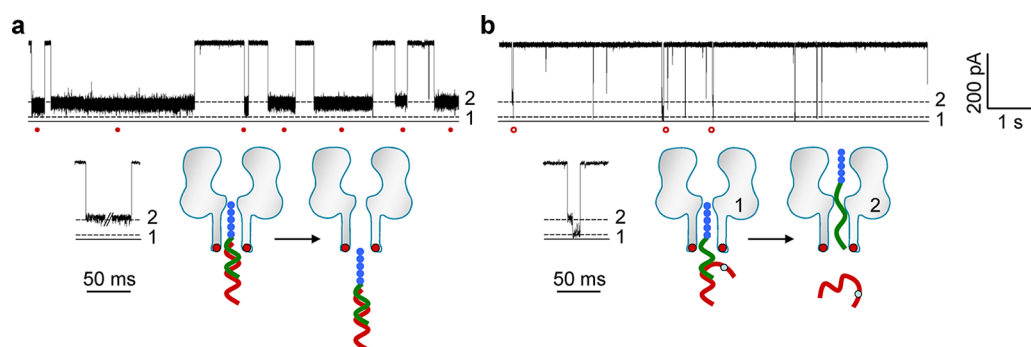
Figure 4. Discrimination of miRNAs with single-nucleotide difference. The probe P_{7b} was used to detect Let-7b and Let-7c. The sequences of the two miRNAs have a single-base difference. The nanopore was monitored at +130 mV in 3 M/0.5 M cis/trans KCl. (a) Current trace showing the long level 2 signatures produced by the fully matched Let-7b•P_{7b} complex. (b) Current traces showing short two-level signatures produced by Let-7c•P_{7b} complex containing one mismatched base pair. The transition from level 2 to level 1 in these signatures suggests the unzipping of the complex in the electrical field.

require accurate discrimination between miRNAs that have similar sequences. Previous work has shown that miRNAs with a single-nucleotide difference can be statistically separated using a DNA probe, based on a 3−4-fold difference in block duration (dehybridization time) between fully matched and one-mismatched miRNA•probe complexes.[21] However, this separation method is not practical in real-time detection because theoretical analysis has indicated that there should be at least 8−10-fold duration difference in order to achieve 90% discrimination accuracy in the mixture.[21] Therefore, we seek to overcome the limitations associated with DNA probes by using PNA. PNAs are a type of artificial nucleic acids which can complimentarily bind to nucleic acids.[49,50] Due to their well-characterized binding strength and specificity, PNAs have been broadly applied in molecular biology, diagnostic assays, and antisense therapies,[50] as well as being used for gene detection in synthetic nanopores.[51] Importantly, it has been demonstrated that a PNA•RNA complex shows higher hybridization strength compared with the same sequence of a DNA•RNA complex.[52] This higher hybridization strength leads to greater specificity in binding to complementary DNAs or RNAs because a PNA/RNA base mismatch is therefore more destabilizing than a similar mismatch in a DNA/RNA duplex.[52] Here we exploit this effect to demonstrate that the use of PNA in the probe can build single-base discrimination capability in the nanopore.

We used probe P_{7b} to target miRNAs Let-7b and Let-7c. Because Let-7c and Let-7b have one nucleotide difference (Table S1), the Let-7c•P_{7b} hybrid contains a single mismatched base pair. Figure 4a shows the current trace for the Let-7b/P_{7b} mixture on the trans side of the pore, monitored at +130 mV in 3 M/0.5 M cis/trans KCl (pH 7.2). The duration of level 2 signatures for fully hybridized Let-7b•P_{7b} was 2.3 ± 0.5 s. When using P_{7b} to detect Let-7c under the same conditions, the number of level 2 signatures was reduced. Instead, the current trace in Figure 4b shows a distinct type of two-level block from level 2 to level 1. These blocks

should be attributed to the unzipping of the Let-7b•P_{7b} complex. Such two-level blocks were rarely observed in Let-7b•P_{7b}, and their duration was 19 ± 7 ms—about 120 times shorter compared with level 2 blocks for Let-7b•P_{7b}. All of these findings suggest that the fully matched miRNA•PNA duplex is sufficiently stable to resist dehybridization, while a single mismatch introduced in the duplex of Let-7c•P_{7b} significantly destabilizes its hybridization. This generates a 120-fold difference in block duration between two miRNAs, and the mismatch-induced unzipping of the complex ensures high-fidelity differentiation of the mismatch from a fully complementary complex. As a result, the current traces for Let-7b and Let-7c can easily be discriminated visually: the long single-step level 2 block with a high occurrence represents Let-7b, and the short two-step block with greatly reduced occurrence represents Let-7c.

This high-fidelity differentiation is also possible even at elevated voltages where dehybridization occurs more frequently. At +180 mV, many of the Let-7b•P_{7b} blocks also featured a level 2−level 1 transition for unzipping. However, the duration of Let-7b•P_{7b} blocks (1.7 ± 0.6 s) was still over 150 times longer than Let-7c•P_{7b} (11 ± 3 ms) (Figure S4). Therefore, both miRNAs can still be accurately discriminated based on the block duration even when unzipping does occur for the Let-7b•P_{7b} blocks.

Enhancing Sensitivity with Optimized Pore and Probe. The integration of probe design and nanopore engineering enables the highly sensitive nucleic acid detection demonstrated above. This high sensitivity is driven in part by the judicious choice of pore mutants and probe designs.

In our K131D mutant pore, the anionic aspartic acid rings constructed at the trans opening of the pore play an important role in attracting cationic molecules, thus greatly increasing the target capture rate k_{on}. For example, the TAT peptide's k_{on} at +180 mV was 4.1 ± 0.9 μM^{-1} s^{-1} in the wild-type pore. The use of K131D vastly elevated the k_{on} over 200-fold to 880 ± 110 μM^{-1} s^{-1} (Figure 5a). Similarly, k_{on} for P_{7b} (peptide-PNA) was enhanced by
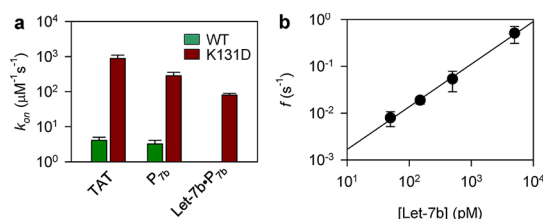
Figure 5. Quantification of miRNAs. (a) Capture rates for the TAT peptide, the probe P_{7b}, and the Let-7b•P_{7b} complex in the wild-type (WT) and K131D pores. (b) Concentration-dependent frequency of Let-7b•P_{7b} signatures in the K131D pore.

90-fold from 3.2 ± 0.9 μM^{-1} s^{-1} in the wild-type pore to 280 ± 70 μM^{-1} s^{-1} in the K131D pore (Figure 5a). Finally, the Let-7b•P_{7b} complex was rarely trapped in the wild-type pore, while its k_{on} was 80 ± 9 μM^{-1} s^{-1} in the K131D pore. We have previously reported that k_{on} for the miRNA in complex with a DNA probe was 1.4 μM^{-1} s^{-1}.[21] Therefore, the combined use of the polycationic probe and the mutant pore enhanced k_{on} over 50-fold. Figure 5b shows that the frequency of Let-7b•P_{7b} signatures consistently increases with increasing Let-7b concentrations ranging from 50 pM to 5 nM at +180 mV. These data can be fitted to a straight line in the log−log scale, which shows that target concentrations lower than 50 pM should be detectable. However, at concentrations that low, the frequency of miRNA signatures would be similar to the spontaneous gating events in the K131D pore[53] ($\sim 6 \times 10^{-3}$ s^{-1} above +140 mV). Fortunately, these gating events can be distinguished from miRNA signatures (Figure S5) and thus can be excluded from events used for miRNA quantification. Recent studies have demonstrated that further structure-directed protein engineering can prevent these intrinsic gate events from occurring,[54,55] providing an approach for future improvement of this system's detection sensitivity.

Concerning our polycationic probe, several key properties of the probe allow us to achieve these critical functions: separate the probe-bound miRNA from free nucleic acids, lead the miRNA•probe complex into the nanopore, and enhance the sensitivity by promoting the capture rate. First, the peptide's sequence and structure are programmable. Its properties can be tuned by adjusting the peptide length and, in particular, the number and position of charged amino acids. The peptide can also be functionalized at both the terminal end and at cysteines in any position of the sequence, making it possible to generate different signatures for multiplex detection. Finally, peptide-PNA probes have the advantage of being synthesized together as their units are all linked by the peptide bond, avoiding additional cross-linking. In future work, we plan to optimize the probe architecture, including net charge count and the charge distribution in order to enhance the capture rate of the miRNA•probe dipole in the pore.

CONCLUSION AND PERSPECTIVE

A polycationic probe can be used for selective nucleic acid detection in the nanopore. While free nucleic acids are electrophoretically driven away from the mouth of the pore, the hybrid of the probe with the target nucleic acids forms a dipole that can be pulled into the asymmetrical electric field at the pore opening. This allows us to selectively detect only those nucleic acid sequences that hybridize with the probe, even when many other confounding species are present.

This result has the potential to be very useful for clinical detection; therefore, the authors are motivated to perform future studies to elucidate the mechanism for the probe-induced nucleic acid separation in an asymmetric electric field, called nanodielectrophoresis. Once the mechanism is determined, we will be able to further optimize and improve our approaches for highly selective and sensitive miRNA detection. If validated in clinical samples, for example, the detection of target miRNA from RNA extractions derived from a patients' biofluids, this method would have applications in many areas such as early disease diagnosis, cancer metastasis prediction, and the monitoring of a patient's response to therapy. In conclusion, this novel approach introduces a new method of detecting clinically relevant DNA or RNA fragments in a complex nucleic acid mixture.

MATERIALS AND METHODS

Chemicals and Materials. Let-7b and Let-7c miRNA oligonucleotides were synthesized and electrophoresis-purified by Integrated DNA Technologies (Coralville, IA). The P_{7b} peptide-PNA probe was synthesized and HPLC-purified by Bio-Synthesis Inc. (Lewisville, TX) with a purity of 95%. All polymers were dissolved in RNAase-free water to 100 μM as stocks. Before the nanopore measurement, the miRNAs, probe, and their mixtures at desired concentrations were heated to 90 °C for 5 min, then gradually cooled to room temperature. Lipid 1,2-diphytanoyl-sn-glycerophosphatidylcholine (DPhPC) was purchased from Avanti Polar Lipids (Alabaster, AL). The 25 μm thick Teflon film was obtained from Goodfellow Inc. (Oakdale, PA). The mutant α-hemolysin proteins K131D and M113R were constructed

according to a method similar to the previous report.[56] The wild-type and mutant proteins were synthesized using the *in vitro* transcription and translation kit provided by Promega Corporation (Madison, WI) and collected from the electrophoresis gel.[57]

Recording of Single-Protein Pores. Nanopore electrical recording was conducted according to previous reports.[21,58] The lipid bilayer membrane was formed over a 100−150 μm orifice in the center of the Teflon film that partitioned between cis and trans recording solutions. Both solutions contained KCl at a desired concentration and were buffered with 10 mM Tris (pH 7.2). The proteins were added in the cis solution, from which they were inserted into the bilayer to form a nanopore. The miRNA and probe polymers were released to the trans solution. The voltage was applied from trans solution and cis solution was grounded,

such that a positive voltage can pull the positively charged probe and miRNA•probe complex into the pore from the trans entrance. The ionic flow through the pore was recorded with an Axopatch 200B amplifier (Molecular Device Inc., Sunnyvale, CA), filtered with a built-in 4-pole low-pass Bessel filter at 5 kHz, and acquired with Clampex 9.0 software (Molecular Device Inc.) through a Digidata 1440 A/D converter (Molecular Device Inc.) at a sampling rate of 20 kHz. Single-channel event amplitude and duration were analyzed using Clampfit 9.0 (Molecular Device Inc.), excel (Microsoft), and SigmaPlot (SPSS) software. The nanopore measurements were conducted at 22 ± 2 °C. Data were presented as mean $\pm$ SD of at least three independent experiments.

Modeling of the miRNA•PNA Duplex. The structure of the miRNA•PNA duplex was estimated using an experimentally determined template (PDB id: 176D); the peptide domain was constructed using the CABS and PULCHRA models[59−61] and the miRNA segment using the Vfold model.[62] The overall structure and charge were calculated from the ensemble average over 20 randomly selected flexible conformations and 100 miRNA conformations in a total of 2000 conformations (Supporting Information S1).

Conflict of Interest: The authors declare no competing financial interest.

Supporting Information Available: Additional experimental details as described in the text. This material is available free of charge *via* the Internet at http://pubs.acs.org.

REFERENCES AND NOTES

1. Bayley, H.; Jayasinghe, L. Functional Engineered Channels and Pores (Review). *Mol. Membr. Biol.* **2004**, *21*, 209–220.

2. Bayley, H.; Cronin, B.; Heron, A.; Holden, M. A.; Hwang, W. L.; Syeda, R.; Thompson, J.; Wallace, M. Droplet Interface Bilayers. *Mol. BioSyst.* **2008**, *4*, 1191–1208.

3. Gu, L. Q.; Shim, J. W. Single Molecule Sensing by Nanopores and Nanopore Devices. *Analyst* **2010**, *135*, 441–451.

4. Hall, A. R.; Scott, A.; Rotem, D.; Mehta, K. K.; Bayley, H.; Dekker, C. Hybrid Pore Formation by Directed Insertion of α-Haemolysin into Solid-State Nanopores. *Nat. Nanotechnol.* **2010**, *5*, 874–877.

5. Hornblower, B.; Coombs, A.; Whitaker, R. D.; Kolomeisky, A.; Picone, S. J.; Meller, A.; Akeson, M. Single-Molecule Analysis of DNA-Protein Complexes Using Nanopores. *Nat. Methods* **2007**, *4*, 315–317.

6. Howorka, S.; Siwy, Z. Nanopore Analytics: Sensing of Single Molecules. *Chem. Soc. Rev.* **2009**, *38*, 2360–2384.

7. Ma, L.; Cockroft, S. L. Biological Nanopores for Single-Molecule Biophysics. *ChemBioChem* **2010**, *11*, 25–34.

8. Majd, S.; Yusko, E. C.; Billeh, Y. N.; Macrae, M. X.; Yang, J.; Mayer, M. Applications of Biological Pores in Nanomedicine, Sensing, and Nanoelectronics. *Curr. Opin. Biotechnol.* **2010**, *21*, 439–476.

9. Movileanu, L. Interrogating Single Proteins through Nanopores: Challenges and Opportunities. *Trends Biotechnol.* **2009**, *27*, 333–341.

10. Olasagasti, F.; Lieberman, K. R.; Benner, S.; Cherf, G. M.; Dahl, J. M.; Deamer, D. W.; Akeson, M. Replication of Individual DNA Molecules under Electronic Control Using a Protein Nanopore. *Nat. Nanotechnol.* **2010**, *5*, 798–806.

11. Venkatesan, B. M.; Bashir, R. Nanopore Sensors for Nucleic Acid Analysis. *Nat. Nanotechnol.* **2011**, *6*, 615–624.

12. Wanunu, M.; Morrison, W.; Rabin, Y.; Grosberg, A. Y.; Meller, A. Electrostatic Focusing of Unlabelled DNA into Nanoscale Pores Using a Salt Gradient. *Nat. Nanotechnol.* **2010**, *5*, 160–165.

13. Wendell, D.; Jing, P.; Geng, J.; Subramaniam, V.; Lee, T. J.; Montemagno, C.; Guo, P. Translocation of Double-Stranded DNA through Membrane-Adapted Phi29 Motor Protein Nanopores. *Nat. Nanotechnol.* **2009**, *4*, 765–772.

14. Langecker, M.; Arnaut, V.; Martin, T. G.; List, J.; Renner, S.; Mayer, M.; Dietz, H.; Simmel, F. C. Synthetic Lipid Membrane Channels Formed by Designed DNA Nanostructures. *Science* **2012**, *338*, 932–936.

15. Branton, D.; Deamer, D. W.; Marziali, A.; Bayley, H.; Benner, S. A.; Butler, T.; Di Ventra, M.; Garaj, S.; Hibbs, A.; Huang, X.; Jovanovich, S. B.; Krstic, P. S.; Lindsay, S.; Ling, X. S.; Mastrangelo, C. H.; Meller, A.; Oliver, J. S.; Pershin, Y. V.; Ramsey, J. M.; Riehn, R.; Soni, G. V.; Tabard-Cossa, V.; Wanunu, M.; Wiggin, M.; Schloss, J. A. The Potential and Challenges of Nanopore Sequencing. *Nat. Biotechnol.* **2008**, *26*, 1146–1153.

16. Cherf, G. M.; Lieberman, K. R.; Rashid, H.; Lam, C. E.; Karplus, K.; Akeson, M. Automated Forward and Reverse Ratcheting of DNA in a Nanopore at 5-Å Precision. *Nat. Biotechnol.* **2012**, *30*, 344–348.

17. Kasianowicz, J. J.; Brandin, E.; Branton, D.; Deamer, D. W. Characterization of Individual Polynucleotide Molecules Using a Membrane Channel. *Proc. Natl. Acad. Sci. U.S.A.* **1996**, *93*, 13770–13773.

18. Manrao, E. A.; Derrington, I. M.; Laszlo, A. H.; Langford, K. W.; Hopper, M. K.; Gillgren, N.; Pavlenok, M.; Niederweis, M.; Gundlach, J. H. Reading DNA at Single-Nucleotide Resolution with a Mutant MspA Nanopore and Phi29 DNA Polymerase. *Nat. Biotechnol.* **2012**, *30*, 349–353.

19. Wallace, E. V.; Stoddart, D.; Heron, A. J.; Mikhailova, E.; Maglia, G.; Donohoe, T. J.; Bayley, H. Identification of Epigenetic DNA Modifications with a Protein Nanopore. *Chem. Commun.* **2010**, *46*, 8195–8197.

20. An, N.; Fleming, A. M.; White, H. S.; Burrows, C. J. Crown Ether–Electrolyte Interactions Permit Nanopore Detection of Individual DNA Abasic Sites in Single Molecules. *Proc. Natl. Acad. Sci. U.S.A.* **2012**, *109*, 11504–11509.

21. Wang, Y.; Zheng, D.; Tan, Q.; Wang, M. X.; Gu, L. Q. Nanopore-Based Detection of Circulating MicroRNAs in Lung Cancer Patients. *Nat. Nanotechnol.* **2011**, *6*, 668–674.

22. Wanunu, M.; Dadosh, T.; Ray, V.; Jin, J.; McReynolds, L.; Drndić, M. Rapid Electronic Detection of Probe-Specific MicroRNAs Using Thin Nanopore Sensors. *Nat. Nanotechnol.* **2010**, *5*, 807–814.

23. Carthew, R. W.; Sontheimer, E. J. Origins and Mechanisms of MiRNAs and SiRNAs. *Cell* **2009**, *136*, 642–655.

24. Lee, R. C.; Feinbaum, R. L.; Ambros, V. The *C. elegans* Heterochronic Gene Lin-4 Encodes Small RNAs with Antisense Complementarity to Lin-14. *Cell* **1993**, *75*, 843–854.

25. Kim, V. N.; Han, J.; Siomi, M. C. Biogenesis of Small RNAs in Animals. *Nat. Rev. Mol. Cell Biol.* **2009**, *10*, 126–139.

26. Wightman, B.; Ha, I.; Ruvkun, G. Posttranscriptional Regulation of the Heterochronic Gene Lin-14 by Lin-4 Mediates Temporal Pattern Formation in *C. elegans*. *Cell* **1993**, *75*, 855–862.

27. Boeri, M.; Verri, C.; Conte, D.; Roza, L.; Modena, P.; Facchinetti, F.; Calabrò, E.; Croce, C. M.; Pastorino, U.; Sozzi, G. MicroRNA Signatures in Tissues and Plasma Predict Development and Prognosis of Computed Tomography Detected Lung Cancer. *Proc. Natl. Acad. Sci. U.S.A.* **2011**, *108*, 3713–3718.

28. Hu, Z.; Chen, X.; Zhao, Y.; Tian, T.; Jin, G.; Shu, Y.; Chen, Y.; Xu, L.; Zen, K.; Zhang, C.; Shen, H. Serum MicroRNA Signatures Identified in a Genome-Wide Serum MicroRNA Expression Profiling Predict Survival of Non-Small-Cell Lung Cancer. *J. Clin. Oncol.* **2010**, *28*, 1721–1726.

29. Hunt, E. A.; Goulding, A. M.; Deo, S. K. Direct Detection and Quantification of MicroRNAs. *Anal. Biochem.* **2009**, *387*, 1–12.

30. Iorio, M. V.; Croce, C. M. MicroRNAs in Cancer: Small Molecules with a Huge Impact. *J. Clin. Oncol.* **2009**, *27*, 5848–5856.

31. Landi, M. T.; Zhao, Y.; Rotunno, M.; Koshiol, J.; Liu, H.; Bergen, A. W.; Rubagotti, M.; Goldstein, A. M.; Linnoila, I.; Marincola, F. M.; Tucker, M. A.; Bertazzi, P. A.; Pesatori, A. C.;

Caporaso, N. E.; McShane, L. M.; Wang, E. MicroRNA Expression Differentiates Histology and Predicts Survival of Lung Cancer. *Clin. Cancer Res.* **2010**, *16*, 430–441.

32. Mitchell, P. S.; Parkin, R. K.; Kroh, E. M.; Fritz, B. R.; Wyman, S. K.; Pogosova-Agadjanyan, E. L.; Peterson, A.; Noteboom, J.; O'Briant, K. C.; Allen, A.; Lin, D. W.; Urban, N.; Drescher, C. W.; Knudsen, B. S.; Stirewalt, D. L.; Gentleman, R.; Vessella, R. L.; Nelson, P. S.; Martin, D. B.; Tewari, M. Circulating MicroRNAs as Stable Blood-Based Markers for Cancer Detection. *Proc. Natl. Acad. Sci. U.S.A.* **2008**, *105*, 10513–10518.

33. Shen, J.; Todd, N. W.; Zhang, H.; Yu, L.; Lingxiao, X.; Mei, Y.; Guarnera, M.; Liao, J.; Chou, A.; Lu, C. L.; Jiang, Z.; Fang, H.; Katz, R. L.; Jiang, F. Plasma MicroRNAs as Potential Biomarkers for Non-Small-Cell Lung Cancer. *Lab Invest.* **2011**, *91*, 579–587.

34. Sozzi, G.; Roz, L.; Conte, D.; Mariani, L.; Andriani, F.; Lo, V. S.; Verri, C.; Pastorino, U. Plasma DNA Quantification in Lung Cancer Computed Tomography Screening: Five-Year Results of a Prospective Study. *Am. J. Respir. Crit. Care Med.* **2009**, *179*, 69–74.

35. Zheng, D.; Haddadin, S.; Wang, Y.; Gu, L. Q.; Perry, M. C.; Freter, C. E.; Wang, M. X. Plasma Micrornas as Novel Biomarkers for Early Detection of Lung Cancer. *Int. J. Clin. Exp. Pathol.* **2011**, *4*, 575–586.

36. Garzon, R.; Calin, G. A.; Croce, C. M. MicroRNAs in Cancer. *Annu. Rev. Med.* **2009**, *60*, 167–179.

37. Ortholan, C.; Puissegur, M. P.; Ilie, M.; Barbry, P.; Mari, B.; Hofman, P. MicroRNAs and Lung Cancer: New Oncogenes and Tumor Suppressors, New Prognostic Factors and Potential Therapeutic Targets. *Curr. Med. Chem.* **2009**, *16*, 1047–1061.

38. Takeshima, K.; Chikushi, A.; Lee, K. K.; Yonehara, S.; Matsuzaki, K. Translocation of Analogues of the Antimicrobial Peptides Magainin and Buforin Across Human Cell Membranes. *J. Biol. Chem.* **2003**, *278*, 1310–1315.

39. Song, L.; Hobaugh, M. R.; Shustak, C.; Cheley, S.; Bayley, H.; Gouaux, J. E. Structure of Staphylococcal α-Hemolysin, a Heptameric Transmembrane Pore. *Science* **1996**, *274*, 1859–1866.

40. Nakane, J.; Wiggin, M.; Marziali, A. A Nanosensor for Transmembrane Capture and Identification of Single Nucleic Acid Molecules. *Biophys. J.* **2004**, *87*, 615–621.

41. Van Dorp, S.; Keyser, U. F.; Dekker, N. H.; Dekker, C.; Lemay, S. G. Origin of the Electrophoretic Force on DNA in Solid-State Nanopores. *Nat. Phys.* **2009**, *5*, 347–351.

42. Luan, B.; Aksimentiev, A. Electric and Electrophoretic Inversion of the DNA Charge in Multivalent Electrolytes. *Soft Matter* **2010**, *6*, 243–246.

43. Meller, A.; Nivon, L.; Branton, D. Voltage-Driven DNA Translocations through a Nanopore. *Phys. Rev. Lett.* **2001**, *86*, 3435–3438.

44. Firnkes, M.; Pedone, D.; Knezevic, J.; Doblinger, M.; Rant, U. Electrically Facilitated Translocations of Proteins through Silicon Nitride Nanopores: Conjoint and Competitive Action of Diffusion, Electrophoresis, and Electroosmosis. *Nano. Lett.* **2010**, *10*, 2162–2167.

45. Maglia, G.; Restrepo, M. R.; Mikhailova, E.; Bayley, H. Enhanced Translocation of Single DNA Molecules through α-Hemolysin Nanopores by Manipulation of Internal Charge. *Proc. Natl. Acad. Sci. U.S.A.* **2008**, *105*, 19720–19725.

46. Gu, L. Q.; Cheley, S.; Bayley, H. Electroosmotic Enhancement of the Binding of a Neutral Molecule to a Transmembrane Pore. *Proc. Natl. Acad. Sci. U.S.A.* **2003**, *100*, 15498–15503.

47. Aksimentiev, A.; Schulten, K. Imaging α-Hemolysin with Molecular Dynamics: Ionic Conductance, Osmotic Permeability, and the Electrostatic Potential Map. *Biophys. J.* **2005**, *88*, 3745–3761.

48. Bhattacharya, S.; Muzard, L.; Payet, L.; Mathe, J.; Bockelmann, U.; Aksimentiev, A.; Viasnoff, V. Rectification of the Current in α-Hemolysin Pore Depends on the Cation Type: The Alkali Series Probed by MD Simulations and Experiments. *J. Phys. Chem. C.* **2011**, *115*, 4255–4264.

49. Nielsen, P. E.; Egholm, M. An Introduction to Peptide Nucleic Acid. *Curr. Issues Mol. Biol.* **1999**, *1*, 89–104.

50. Nielsen, P. E.; Shiraishi, T. Peptide Nucleic Acid (PNA) Cell Penetrating Peptide (CPP) Conjugates as Carriers for Cellular Delivery of Antisense Oligomers. *Artif. DNA* **2011**, *2*, 90–99.

51. Singer, A.; Wanunu, M.; Morrison, W.; Kuhn, H.; Frank-Kamenetskii, M.; Meller, A. Nanopore Based Sequence Specific Detection of Duplex DNA for Genomic Profiling. *Nano Lett.* **2010**, *10*, 738–742.

52. Natsume, T.; Ishikawa, Y.; Dedachi, K.; Tsukamoto, T.; Kurita, N. Hybridization Energies of Double Strands Composed of DNA, RNA, PNA and LNA. *Chem. Phys. Lett.* **2007**, *434*, 133–138.

53. Mohammad, M. M.; Movileanu, L. Impact of Distant Charge Reversals within a Robust β-Barrel Protein Pore. *J. Phys. Chem. B* **2010**, *114*, 8750–8759.

54. Mohammad, M. M.; Iyer, R.; Howard, K. R.; McPike, M. P.; Borer, P. N.; Movileanu, L. Engineering a Rigid Protein Tunnel for Biomolecular Detection. *J. Am. Chem. Soc.* **2012**, *134*, 9521–9531.

55. Chen, M.; Khalid, S.; Sansom, M. S.; Bayley, H. Outer Membrane Protein G: Engineering a Quiet Pore for Biosensing. *Proc. Natl. Acad. Sci. U.S.A.* **2008**, *105*, 6272–6277.

56. Howorka, S.; Bayley, H. Improved Protocol for High-Throughput Cysteine Scanning Mutagenesis. *BioTechniques* **1998**, *25*, 764–770.

57. Shim, J. W.; Yang, M.; Gu, L. Q. *In Vitro* Synthesis, Tetramerization and Single Channel Characterization of Virus-Encoded Potassium Channel Kcv. *FEBS Lett.* **2007**, *581*, 1027–1034.

58. Shim, J. W.; Tan, Q.; Gu, L. Q. Single-Molecule Detection of Folding and Unfolding of the G-Quadruplex Aptamer in a Nanopore Nanocavity. *Nucleic Acids Res.* **2009**, *37*, 972–982.

59. Kolinski, A. Protein Modeling and Structure Prediction with a Reduced Representation. *Acta Biochim. Pol.* **2004**, *51*, 349–371.

60. Kolinski, A.; Skolnick, J. Reduced Models of Proteins and Their Applications. *Polymer* **2004**, *45*, 511–524.

61. Rotkiewicz, P.; Skolnick, J. Fast Procedure for Reconstruction of Full-Atom Protein Models from Reduced Representations. *J. Comput. Chem.* **2008**, *29*, 1460–1465.

62. Cao, S.; Chen, S. J. Predicting RNA Folding Thermodynamics with a Reduced Chain Representation Model. *RNA* **2005**, *11*, 1884–1897.